ACS Catalysis

pubs.acs.org/acscatalysis

Letter

Electrochemical CO_2 Reduction to Methanol by Cobalt Phthalocyanine: Quantifying CO_2 and CO Binding Strengths and Their Influence on Methanol Production

Libo Yao,[#] Kevin E. Rivera-Cruz,[#] Paul M. Zimmerman,* Nirala Singh,* and Charles C. L. McCrory*

Cite This: ACS Catal. 2024, 14, 366–372

Read Online

ACCESS | Metrics & More | Article Recommendations | Supporting Information

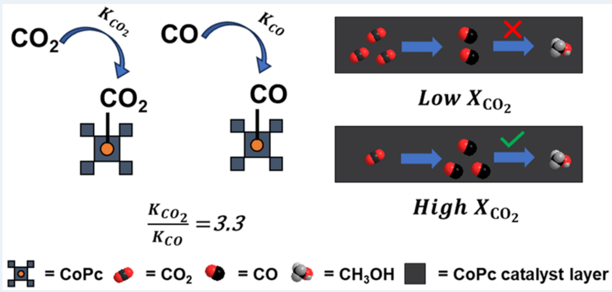

ABSTRACT: Cobalt phthalocyanine (CoPc) is an active electrocatalyst for the sequential electrochemical reductions of CO_2-to-CO and CO-to-methanol (CH_3OH), and it has been shown to be active for the conversion of CO_2-to-CH_3OH through a cascade catalysis reaction. However, in gas-fed flow electrolyzers equipped with gas diffusion electrodes (GDEs), the reduction of CO_2 by CoPc selectively produces CO with minimal CH_3OH formation. Herein, we show that the limited performance of the CO_2−CO−CH_3OH cascade reactions by CoPc is primarily due to the competitive binding between the CO_2 and CO species. Through microkinetic analyses, we determine that the effective equilibrium constant for CO_2 binding is three times higher than that for CO binding. The stronger CO_2 binding suppresses the CO-to-CH_3OH reaction even at moderate local CO_2 concentrations. Because the GDE configuration enhances the CO_2 mass transport, gas-fed flow electrolyzers exacerbate this suppression of CH_3OH formation from the CO_2RR. In contrast, CH_3OH formation is observed when the local concentration of the CO_2 is low, compared to the local CO concentration. To promote methanol formation via CO_2 reduction, we propose applying modifications to the coordination environments of CoPc to strengthen the binding of CO and regulate the transport of CO_2.

KEYWORDS: *Electrochemical CO_2 reduction, methanol synthesis, cobalt phthalocyanine, competitive CO_2 and CO binding, DFT calculations*

INTRODUCTION

The electrochemical CO_2 reduction reaction (CO_2RR) to produce value-added chemicals holds great promise for carbon recycling and energy storage.[1−3] CO_2RR to highly reduced products like methanol (CH_3OH) is of particular interest, because CH_3OH is a critical chemical building block and promising energy storage molecule.[4,5] However, designing catalyst systems for the selective CO_2RR to products that require more than two-electron transfers is challenging due to the complexity of reaction pathways and the limited understanding of the reaction mechanisms.[6−9] Therefore, the six-electron reduction of CO_2 to CH_3OH often suffers from sluggish reaction kinetics and poor selectivity.[9]

Using immobilized molecular catalysts (IMCs) that are adsorbed or grafted on conductive carbon supports provides promising model systems to understand reaction mechanisms and control the kinetics and selectivity. IMCs not only provide single-atom active sites that suppress competitive C−C coupling reactions,[10,11] but also offer precise control over catalytic performance at a mechanistic level due to their tunable electronic properties and microenvironments.[8,12−15] Early examples of molecular transition-metal complexes for CO_2-to-CH_3OH reactions include Co-, Fe-, Ni-, and Cr-based molecular catalysts that are aided by heterogeneous and homogeneous co-catalysts to facilitate the production of CH_3OH in organic solvents.[16,17] However, perhaps the most prevalent examples of the CO-to-CH_3OH by IMCs in *aqueous* electrolyte emerged in 2019. Robert and co-workers[18,19] and Wang and co-workers[20] independently reported that cobalt phthalocyanine immobilized on multi-walled carbon nanotubes (CoPc/MWCNT), which is a catalyst known for its selectivity for the CO_2-to-CO reaction, exhibited activity in an aqueous H-type cell (H-cell) for the reduction of CO_2 to CH_3OH. CH_3OH formation is proposed to occur through a CO_2−CO−CH_3OH cascade reaction with CO acting as the intermediate.[18−21] Further studies have demonstrated that formaldehyde is a likely intermediate for the CO-to-CH_3OH reaction[19] and higher Faradaic efficiencies for CH_3OH (FE_{CH_3OH}) are achieved from the four-electron CO-to-CH_3OH reaction than the six-electron CO_2-to-CH_3OH reaction.[18]

Received: October 16, 2023
Revised: November 20, 2023
Accepted: December 8, 2023
Published: December 19, 2023

https://doi.org/10.1021/acscatal.3c04957
ACS Catal. 2024, 14, 366−372

Although CoPc/MWCNT can catalyze the CO_2−CO−CH_3OH cascade reaction, the rates and CH_3OH selectivity remain low, compared to state-of-the-art solid-state CO_2−CH_3OH electrocatalysts.[22−24] Moreover, incorporating the CoPc/MWCNT into gas-fed flow electrolyzers makes this CO_2−CO−CH_3OH performance even worse, compared with the equivalent systems studied in aqueous H-cells. For example, Wang and co-workers reported an average CO_2−CO−CH_3OH current density (j_{CH3OH}) of <10 mA/cm^2 and a FE_{CH3OH} value of ∼40% in H-cell configuration.[20] However, CoPc-based gas-diffusion electrodes (GDEs) have shown CO_2-to-CO current densities (j_{CO}) of hundreds of mA/cm^2 and almost 100% CO Faradaic efficiency (FE_{CO}),[11,25−29] but CH_3OH has rarely been detected in the numerous flow electrolyzer studies published in recent years. One recent exception has been reported by Ye and co-workers, in which they achieved j_{CH3OH} > 60 mA/cm^2 under >30% FE_{CH3OH} in a GDE by engineering the strain effects of single-walled carbon nanotubes.[30] In contrast to the low CH_3OH production from CO_2 in GDEs, the direct CO reduction reaction (CORR) by CoPc is active and selective for CH_3OH production. Multiple reports demonstrate CORR performance with 20−90 mA/cm^2 j_{CH3OH} and >65% FE_{CH3OH} in zero-gap flow electrolyzers.[30,31]

The contrast in CH_3OH production by CoPc under the CO_2RR and CORR conditions suggests that CO-to-CH_3OH is largely suppressed by the presence of CO_2. The suppression is closely related to the relative binding strength of CO and CO_2 to CoPc.[31] In more recent studies, Wang and co-workers pointed out that the bound CO species (*CO) is labile on CoPc sites and high *CO concentration in the microenvironment is necessary to compete with CO_2 in order to facilitate CH_3OH formation.[32] However, a gap in the literature is a quantitative understanding of CO and CO_2 binding and how the difference in binding influences the formation of CH_3OH on CoPc. This knowledge gap may hinder future optimization studies aiming at scaling up CH_3OH production.[33] Therefore, the objective of this study is to quantify binding of CO and CO_2 to CoPc and elucidate how the relative CO_2/CO binding impacts the CO_2−CO−CH_3OH reaction by CoPc/MWCNT catalysts in gas-fed flow electrolyzers.

COMPARING CO_2 AND CO BINDING CONSTANTS TO COPC/MWCNT CATALYST

To quantitatively compare the relative binding for CO and CO_2 to CoPc/MWCNT, we measured the CORR and CO_2RR activity of CoPc/MWCNTs in our gas-fed flow electrolyzer where the feed gas stream had different partial pressures of CO (P_{CO}) and CO_2 (P_{CO2}), respectively, balanced by N_2. The results of these experiments were fitted to a microkinetic reaction model to determine the equilibrium binding constants for CO and CO_2 to CoPc (denoted as K_{CO} and K_{CO2}, respectively). Details of the flow electrolyzer and reaction methods are provided in Section 1 in the Supporting Information and Figure S1 in the Supporting Information. In addition to the flow electrolyzer studies, we conducted H-cell electrolysis for CO_2RR and CORR with CoPc/MWCNT to determine whether our catalyst is comparable with the reported state-of-the-art performance in aqueous non-flowing H-cells. The experimental methods are detailed in Section 1 in the Supporting Information, and the results of electrolysis are shown in Figure S2 in the Supporting Information. For the CO_2RR, we saw an onset of CH_3OH formation at approximately − 0.70 V vs RHE with 1.4% FE_{CH3OH}. Under a more negative potential of −0.85 V vs RHE FE_{CH3OH} reaches 11.7%. For the CORR, 7.4% and 24.1% FE_{CH3OH} is achieved at the aforementioned potentials. When taking the difference of reactor and reaction conditions into consideration, the CH_3OH production in our sealed H-cell is qualitatively comparable with the state-of-the-art performance reported with CoPc/MWCNT catalysts under similar reaction conditions.[20,30]

To determine K_{CO}, we studied the CORR by CoPc/MWCNT at different inlet P_{CO} values. First, we determined the optimal operating potential for CH_3OH formation from the CORR on a CoPc/MWCNT GDE with 1 atm of CO in our gas-fed flow electrolyzer. We observe that CH_3OH formation commences at a potential of approximately −0.44 V vs RHE and reaches its peak at approximately −0.77 V (Figures S3 and S4 in the Supporting Information). At this peak potential, j_{CH3OH} = −44.7 mA/cm^2. CH_3OH is most selectively generated at −0.70 V vs RHE with FE_{CH3OH} > 80%. We therefore used the potential of −0.70 V vs RHE to measure j_{CH3OH} as a function of P_{CO} for the CORR. As shown in Figure 1a and Figure S5, j_{CH3OH} increases with CO partial pressure until it plateaus at P_{CO} = 1 atm, and we attribute this plateau to saturated CO binding. Using microkinetic analyses detailed in Section 2 in the Supporting Information, we determined that the rate-determining step (RDS) for the conversion of CORR to methanol to be the protonation of [CO-CoPc]$^-$, which

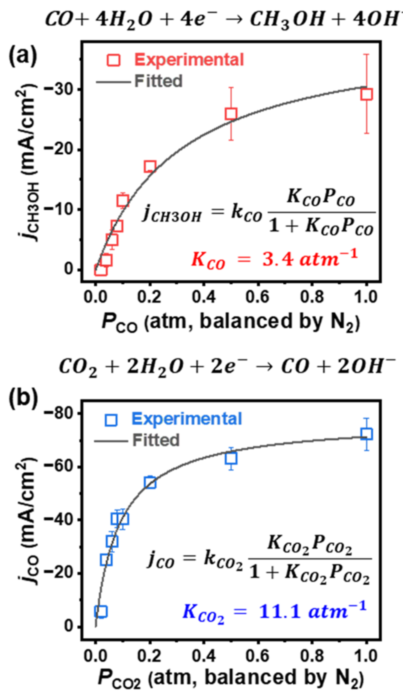

Figure 1. Current density to specified product as a function of inlet partial pressure of reactant for (a) CO-to-methanol (j_{CH_3OH}, mA/cm^2) and (b) CO_2-to-CO (j_{CO}, mA/cm^2) using CoPc/CNT catalyst. All electrochemical measurements are conducted in a flow electrolyzer under −0.7 V vs RHE with 0.5 M $KHCO_3$ electrolyte (pH ∼8.5). Both the CO and CO_2 gases are balanced by N_2 to 1 atm with total gas flow rate controlled at 15 mL/min. Experimental results are shown by data points from three repetitions, fitting is shown by a solid line. The numerical fitting was done by using the equation shown and derived in Section 2 in the Supporting Information. The effective equilibrium constants for CO (K_{CO}) and CO_2 (K_{CO2}) binding to CoPc are obtained from the fitted results.

https://doi.org/10.1021/acscatal.3c04957
ACS Catal. 2024, 14, 366−372

represents the CO-bound, singly reduced CoPc molecule. The RDS determined from our microkinetic analysis is in agreement with the recent kinetic studies in aqueous H-cell by Wang and co-workers.[34] Using this RDS, we derived a rate law for CH_3OH production from CO shown in eq 1.

$$j_{CH3OH} = k_{CO}\left(\frac{K_{CO}P_{CO}}{1 + K_{CO}P_{CO}}\right) \quad (1)$$

k_{CO} refers to an effective rate constant for the CORR to CH_3OH as defined in Section 2 in the Supporting Information and K_{CO} is the apparent equilibrium binding constant to the CoPc/MWCNT catalyst. By numerically fitting the experimental j_{CH3OH} data in Figure 1a to eq 1, we determined K_{CO} = 3.4 atm^{-1}.

We conducted analogous studies of the CO_2RR by CoPc/MWCNT at different P_{CO2} to determine K_{CO2} at −0.7 V vs RHE. The primary products for the CO_2RR with CoPc catalyst are CO and H_2, with minimal CH_3OH produced. The relationship between j_{CO} from the CO_2RR as a function of P_{CO2} is shown in Figure 1b. j_{CO} increases with increasing CO_2 partial pressure until it plateaus at $P_{CO2} \approx 0.8-1.0$ atm, qualitatively similar to the relationship between j_{CH3OH} and P_{CO} in Figure 1a. We applied a similar microkinetic analysis to derive a rate law for CO production from CO_2 assuming protonation of the $[CO_2-CoPc]^-$ species is the RDS shown in eq 2.

$$j_{CO} = k_{CO2}\left(\frac{K_{CO2}P_{CO2}}{1 + K_{CO2}P_{CO2}}\right) \quad (2)$$

Similarly, k_{CO2} refers to an effective rate constant for the CO_2RR to CO and K_{CO2} is the apparent equilibrium binding constant to the CoPc/MWCNT catalyst. By fitting the j_{CO} data in Figure 1b to eq 2, we determined K_{CO2} = 11.1 atm^{-1}.

Note that the various assumptions used in these microkinetic models and data fitting are described in Section 2 in the Supporting Information, and the MATLAB code used for fitting and the statistical significance of the fitted results are shown in Section 3 in the Supporting Information. The $j-P$ relationships shown in Figures 1a and b demonstrate a correlation between the current density and the bulk concentration of reactants, while it is the local concentration that intrinsically determines the reaction rate. By fitting our rate laws derived from microkinetic analysis to P-dependent experimental trends to derive equilibrium binding constants for the purpose of comparing relative binding strengths for CO and CO_2, we are implicitly assuming that (1) the local CO or CO_2 concentration is a regular function of the measured P_{CO} and P_{CO2} pressures, and (2) equilibrium of CO and CO_2 binding is rapidly achieved at any given P_{CO} and P_{CO2}. If valid, then these assumptions mean that these apparent K_{CO} and K_{CO2} values provide important insights into the relative ability of CoPc/MWCNTs to bind CO_2 and CO.

The ratio of the equilibrium binding constants extracted from kinetic fitting is K_{CO2}/K_{CO} = 3.3, implying that binding of CO_2 to the CoPc catalyst is stronger, compared to that of CO binding. This insight provides a thermodynamic explanation for the inefficient CH_3OH formation on CoPc/MWCNTs during the CO_2RR. Under most conditions, as CO_2 is converted to CO, the CO is preferentially displaced by a CO_2 molecule before the CO can be further protonated to produce CH_3OH. In other words, we postulate that CH_3OH formation is suppressed by the presence of CO_2 through competitive binding of CO_2 at the catalyst active sites.

■ COMPUTATIONAL STUDIES OF CO AND CO_2 BINDING AT COPC

To understand better the atomistic behavior of the CO and CO_2 binding, we performed density functional theory (DFT) calculations using quantum mechanics/molecular mechanics models of CoPc and explicit solvent, as detailed in Section 4 in the Supporting Information. The CORR and CO_2RR pathways investigated by DFT are shown in Figure 2a. The binding of

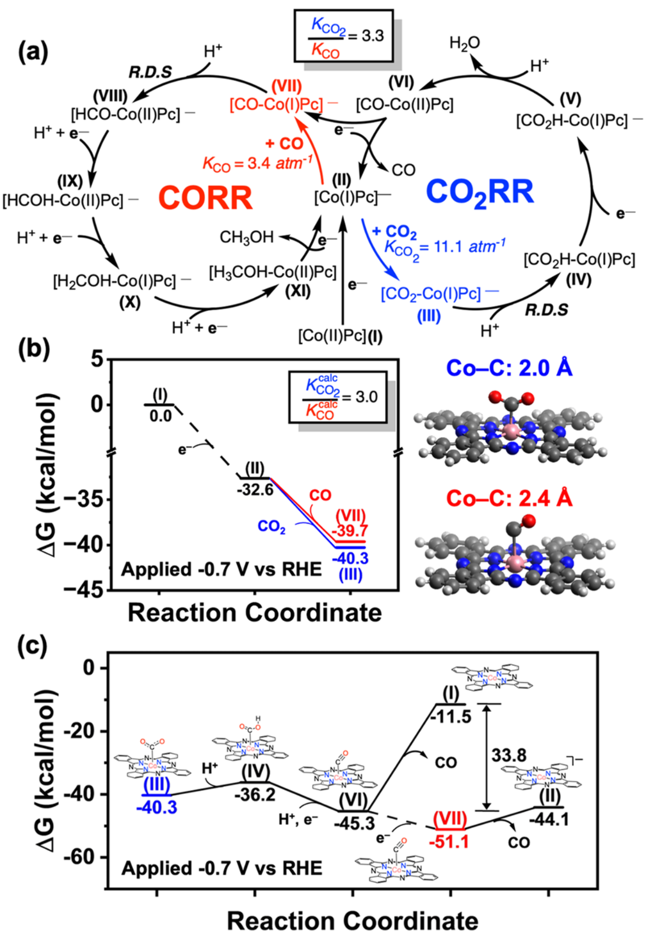

Figure 2. (a) Proposed reaction mechanism for CO_2-to-CO and CO-to-CH_3OH on CoPc/CNT under −0.7 V vs RHE applied potential. (b) Calculated Gibbs free energy for the binding of CO and CO_2 on singly reduced Co(I)Pc intermediate. (c) Calculated Gibbs free energy for the CO_2−CO reduction reaction on CoPc catalyst. All electron reduction events are referenced to the experimentally applied −0.7 V vs RHE potential. Structures show graphical representations of the optimized $[CO_2-CoPc]^-$ (Intermediate III) and $[CO\text{-}CoPc]^-$ (Intermediate VII) systems. [Legend: pink sphere = Co, blue sphere = N, gray sphere = C and white sphere = H.]

CO_2 to singly reduced CoPc, i.e., $[CO_2-CoPc]^-$, has a more favorable Gibbs free energy (ΔG_{CO_2} = −7.6 kcal/mol, Figure 2b, Intermediate III) than its CO-bound counterpart ($[CO\text{-}CoPc]^-$, ΔG_{CO} = −7.0 kcal/mol, Figure 2b, Intermediate VII). This difference between ΔG_{CO2} and ΔG_{CO} equates to a ratio of equilibrium binding constants of $K^{calc}_{CO2}/K^{calc}_{CO}$ = 3.0 (see Section 3 in the Supporting Information), which agrees well with the experimentally obtained $K_{CO2)}/K_{CO}$ = 3.3.

https://doi.org/10.1021/acscatal.3c04957
ACS Catal. 2024, 14, 366−372

Having computational support for the preferential binding of CO_2 over CO, we studied the key reaction intermediates for the reduction of CO_2 to CO under the applied potential of −0.7 V vs RHE (Figure 2c). After binding of CO_2 to the singly reduced CoPc active site, protonation of the CO_2 adduct is uphill by 4.1 kcal/mol (Figure 2c, III → IV). The protonated CO_2 adduct, however, can be reduced by proton-coupled electron transfer (Figure 2c, IV → VI) that generates CO bound to neutral CoPc and is downhill from the IV ion by −9.1 kcal/mol. While direct desorption of the CO adduct from VI is highly unfavorable thermodynamic (33.8 kcal/mol; Figure 2c, VI → I), the reduction of the [CO-CoPc] intermediate at −0.7 V vs RHE is favorable (VI → VII). The singly reduced CoPc species releases CO at a cost of only 7.0 kcal/mol (Figure 2c, Step VII → II). This suggests that desorption of the CO adduct is enabled by reduction of the neutral [CO-CoPc] intermediate (Figure 2c, VII), which regenerates the singly reduced CoPc species. (Figure 2c, II) It is worth noting that further protonation of $[CO\text{-}CoPc]^-$ to form [HCO-CoPc] is possible, but our microkinetic analysis as well as recent studies reveal the protonation of $[CO\text{-}CoPc]^-$ is a likely RDS for CH_3OH formation,[32,35] therefore making this route difficult to compete with CO_2 replacement. Altogether, these results suggest that the stronger binding of CO_2, compared to that of CO on singly reduced CoPc, is responsible for the reduced methanol activity observed in the experiment.

■ STUDYING THE COMPETITIVE INHIBITION OF CORR BY CO_2

Our studies above provided experimental and computational evidence that CoPc/MWCNT has a stronger binding affinity for CO_2 compared to CO, and computational mechanistic analysis suggested that this stronger binding affinity for CO_2 inhibits CH_3OH formation during the CO_2RR. To verify this competitive inhibition by CO_2, we studied the activity of CoPc/MWCNT for CH_3OH production in a series of CO/CO_2 cofeeding experiments in a gas-fed flow electrolyzer. Here, we varied P_{CO} while balancing by P_{CO2} to achieve a total inlet pressure of 1 atm. The results of these experiments are shown in Figures 3a and 3b, and Figure S5. Importantly, CH_3OH is detected as a product only when $P_{CO} \geq 0.9$ atm ($P_{CO2} \leq 0.1$ atm). At all partial pressures of $P_{CO} < 0.9$ atm and corresponding $P_{CO2} > 0.1$ atm, CO is the only C-containing product. This result is quantitatively consistent with similar studies by Liu and co-workers conducted in a non-flow aqueous H-cell.[31] We interpret this result to mean that the partial pressure of CO must be sufficiently high relative to CO_2 for CO to bind to the catalyst and react to form CH_3OH. In comparison, when CO_2 was substituted with N_2, CH_3OH forms at a much lower P_{CO} of 0.02 atm (Figure 1a)—N_2 does not competitively inhibit CH_3OH, whereas CO_2 does. Moreover, at any given P_{CO}, j_{CH3OH} and FE_{CH3OH} are much higher in the CO/N_2 mixture than in the CO/CO_2 mixture (see Figures 3a and b, as well as Figure S6 in the Supporting Information). The difference in j_{CH3OH} achieved in the CO/N_2 and CO/CO_2 mixtures diminishes when P_{CO} approaches 1 atm.

We conducted further verification of the suppression of CH_3OH by CO_2 on CoPc/MWCNT with ^{13}C isotope labeling experiments. We hypothesize that the $^{13}CO_2$ has weaker binding to CoPc, compared to its ^{12}C isotopologue, resulting in less-severe suppression on methanol formation via CORR. This hypothesis is supported by the carbon isotope

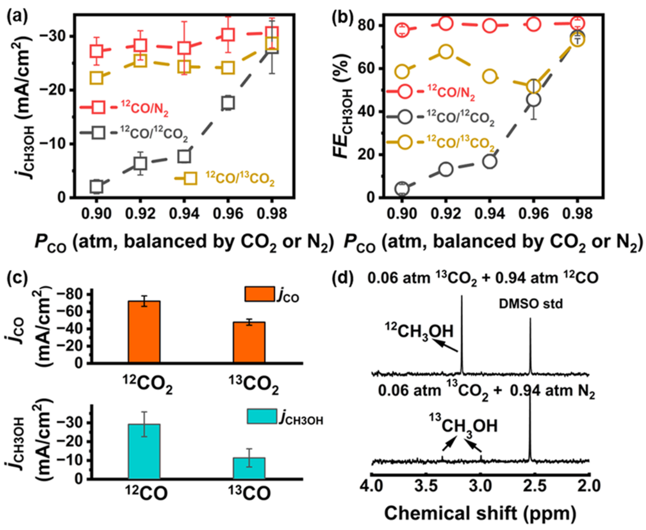

Figure 3. (a) j_{CH3OH} and (b) FE_{CH3OH} under different gas mixtures for CoPc/MWCNT catalyst at −0.7 V vs RHE. The gas mixtures include ^{12}CO balanced by N_2 (red), ^{12}CO balanced by $^{12}CO_2$ (black), and ^{12}CO balanced by $^{13}CO_2$ (yellow). (c) Performance of CO_2R (j_{CO}, orange) and CORR (j_{CH3OH}, blue) using ^{12}C and ^{13}C isotopologues with 1 atm CO_2 or CO gases. (d) ^1H NMR spectra for the liquid products collected with 0.06 atm $^{13}CO_2$ + 0.94 atm ^{12}CO (upper panel), and 0.06 atm $^{13}CO_2$ + 0.94 atm N_2 (lower panel) gas mixtures. All electrochemical measurements are conducted in a flow electrolyzer under −0.7 V vs RHE with 0.5 M $KHCO_3$ electrolyte (pH ∼8.5).

discrimination phenomenon observed in photosynthesis, where the $^{13}C/^{12}C$ ratios in the products are lower than that of CO_2 in nature.[36] This phenomenon has been identified in CO_2RR.[37] We performed ^{13}C-labeled CO_2RR and CORR. We observed noticeable decreases in j_{CO} and j_{CH3OH} when using 1 atm of $^{13}CO_2$ and ^{13}CO, compared with their ^{12}C isotopologues (see Figure 3c, as well as Figures S7 and S8 in the Supporting Information). Note that $^{13}CO_2$RR produces only ^{13}CO while ^{13}CORR only generates $^{13}CH_3OH$. We further conducted cofeeding experiments with $^{12}CO/^{13}CO_2$ mixtures, and the j_{CH3OH} and FE_{CH3OH} values for the $^{12}CO/^{13}CO_2$ mixtures are similar to the $^{12}CO/N_2$ mixtures, as shown in Figures 3a and b. This suggests the $^{13}CO_2$ did not suppress the CO-to-methanol reaction as much as its ^{12}C isotopologue, supporting our hypothesis that the more weakly bound $^{13}CO_2$ has less suppression of the CO-to-CH_3OH reaction. Note that the interpretation of the ^{13}C isotope labeling experiments is conducted under two key hypotheses: (1) the ^{13}C discrimination observed in electrochemical CO_2 reduction applies to CoPc catalyst systems, and (2) the binding strength of CO_2 is positively correlated with the CO_2RR performance on CoPc. Both hypotheses are supported by previous studies,[13,15,37] but the slower kinetics of certain $^{13}CO_2$RR and ^{13}CORR reaction steps is a possible contributing factor that cannot be completely ruled out.

While our results demonstrate the suppression of CH_3OH formation in the presence of CO_2 at the catalyst active sites, we show that CH_3OH can still be produced via the CO_2RR if the local CO_2 is sufficiently consumed. For the P_{CO2}-dependent CO_2RR shown in Figures 4a and b, the performance of the CO_2RR declines due to limited CO_2 mass transport. This trend is more pronounced when P_{CO2} is between 0.02 and 0.1 atm, where a linear correlation between j_{CO} and P_{CO2} is observed, indicating that the reaction rate is predominantly controlled by

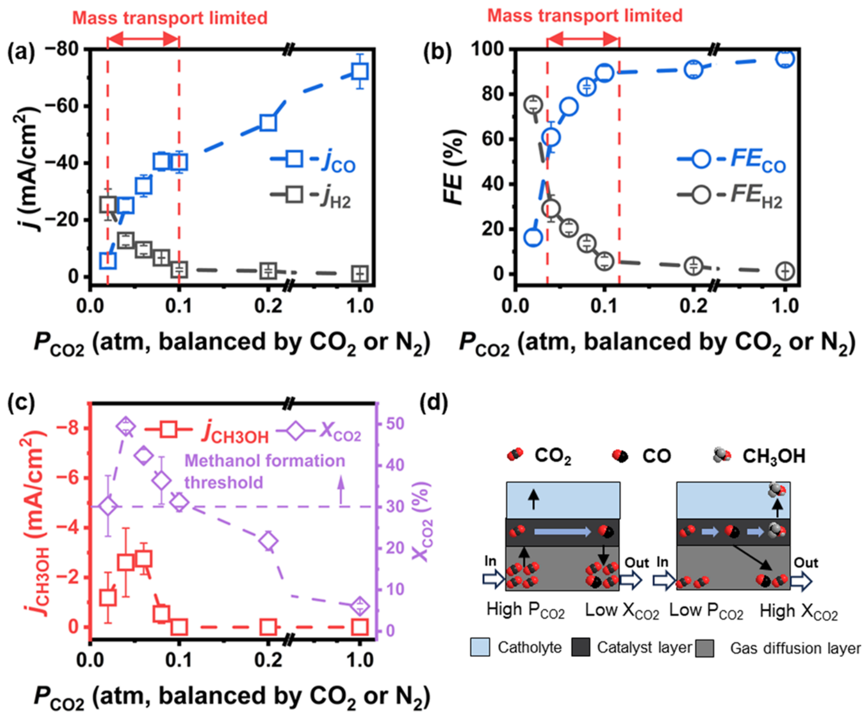

Figure 4. (a) Current densities and (b) Faradaic efficiencies to CO and H_2, as a function of P_{CO_2}. (c) CH_3OH current density (j_{CH3OH}) and CO_2 single pass conversion (X_{CO2}, %) as a function of P_{CO_2}. CO_2 conversion of >30% coincides with CH_3OH formation. CO_2 gas is balanced by N_2 to 1 atm with total gas flow rate controlled at 15 mL/min. All reactions were conducted in a flow electrolyzer under chronoamperometry mode with −0.7 V vs RHE applied potential. (d) Schematic illustration of the relationship among P_{CO2}, X_{CO2}, and CH_3OH formation. When high P_{CO2} is fed (left side image), there is low X_{CO2} and high CO_2 concentration within catalyst layer, and no methanol is formed. When low P_{CO2} is fed (right side image), a higher fraction of CO_2 is converted and the CO/CO_2 ratio becomes sufficiently high at the catalyst layer to produce CH_3OH.

mass transport of CO_2 rather than the intrinsic kinetics of the catalyst. CH_3OH is detected within the same P_{CO_2} range (Figure 4c), suggesting that CH_3OH formation is "switched on" when the CO_2RR is limited by the CO_2 mass transport. Additionally, we observe a strong correlation between the single-pass conversion of CO_2 (X_{CO2}) and CH_3OH formation. The decrease in P_{CO2} results in higher X_{CO2}, and higher X_{CO2} leads to the formation of CH_3OH. A threshold of 30% X_{CO2} is required in our case for methanol formation from the CO_2−CO-methanol route (Figure 3c). The high X_{CO2} value required to generate methanol suggests the need to establish a CO_2 "lean" or "depleted" local environment to minimize the CO_2 competition (Figure 4d). Based on this rationale, we identify the main reason for the absence of methanol formation via the CO_2RR in most flow electrolyzer studies using CoPc-based catalysts. The use of pure or high partial pressure CO_2 gas enables a high CO_2 volumetric flow rate that leads to low X_{CO_2}, which, combined with fast CO_2 transport, results in a high CO_2 concentration near the catalyst active site. This high local CO_2 concentration significantly suppresses the CO−methanol pathway due to the preferential binding of CO_2, compared to CO.

CONCLUSIONS

In conclusion, we study the relative binding strength of CO_2 and CO to CoPc and its influence on CH_3OH formation through the CO_2RR. We find that CO_2 exhibits stronger binding to CoPc than CO, leading to the suppression of the CO−CH_3OH reaction during the CO_2−CO−CH_3OH cascade. We determine that the effective equilibrium constant for CO_2 binding (K_{CO2}, 11.1 atm^{-1}) is more than 3 times higher than that for CO binding (K_{CO}, 3.4 atm^{-1}), resulting in an unfavorable CO−CH_3OH reaction when CO_2 is present near the catalyst at appreciable concentrations. The use of flow electrolyzers exacerbates the suppression of CH_3OH due to the significantly improved CO_2 mass transport, which maintains high local CO_2 concentrations. To enhance CH_3OH formation via the CO_2RR, future studies can target catalyst design and control of the catalyst microenvironment. Catalyst design should aim at addressing the weaker binding of CO. Rational ligand modifications on CoPc should be investigated to enhance the level of binding of CO, with a specific emphasis on decreasing the K_{CO2}/K_{CO} ratio. Additionally, control of local concentrations (i.e., the relative ratio of CO_2 and CO concentrations near the catalyst) can be achieved through the construction of catalyst−polymer composites, where the polymers effectively modulate the local CO_2 concentration in the microenvironment.[12,28,38] Successful implementation of these strategies could effectively improve CH_3OH production via the CO_2−CO−CH_3OH route with CoPc-based catalysts.

ASSOCIATED CONTENT

Supporting Information

The Supporting Information is available free of charge at https://pubs.acs.org/doi/10.1021/acscatal.3c04957.

Additional information including materials and experimental methods; full computational description of the implicit solvated catalyst structure, description of the quantum mechanics/molecular mechanics model; tables including the electronic, solvated and frequency corrected energies for all intermediates studied; derivation of the microkinetic models; MATLAB codes

https://doi.org/10.1021/acscatal.3c04957
ACS Catal. 2024, 14, 366−372

for the numerical fitting; exploded view of flow electrolyzer; results for potential-dependent CO reduction; supplementary CORR and CO_2RR results under different partial pressures; ^{1}H NMR and electrolysis results for the ^{13}C labeling experiments (PDF)

■ AUTHOR INFORMATION

Corresponding Authors

Paul M. Zimmerman − *Department of Chemistry, University of Michigan, Ann Arbor, Michigan 48109, United States;* orcid.org/0000-0002-7444-1314; Email: paulzim@umich.edu

Nirala Singh − *Department of Chemical Engineering, University of Michigan, Ann Arbor, Michigan 48109, United States;* orcid.org/0000-0003-0389-3927; Email: snirala@umich.edu

Charles C. L. McCrory − *Department of Chemistry and Macromolecular Science & Engineering Program, University of Michigan, Ann Arbor, Michigan 48109, United States;* orcid.org/0000-0001-9039-7192; Email: cmccrory@umich.edu

Authors

Libo Yao − *Department of Chemical Engineering and Department of Chemistry, University of Michigan, Ann Arbor, Michigan 48109, United States;* orcid.org/0000-0001-7183-529X

Kevin E. Rivera-Cruz − *Department of Chemistry, University of Michigan, Ann Arbor, Michigan 48109, United States;* orcid.org/0000-0001-6690-1571

Complete contact information is available at: https://pubs.acs.org/10.1021/acscatal.3c04957

Author Contributions

#L.Y. and K.E.R.-C. contributed equally to this work. N.S., C.C.L.M., and L.Y. conceived the project. L.Y. carried out all the experiments. K.E.R.-C. performed DFT calculations. P.M.Z. provided supervision of computational studies. L.Y. and K.E.R.-C. drafted the manuscript. All authors were involved in revising the manuscript and gave approval to the final version.

Notes

The authors declare no competing financial interest.

■ ACKNOWLEDGMENTS

We thank the Carbon Neutrality Acceleration Program (CNAP) from Graham Sustainability Institute in University of Michigan for providing funding support. C.C.L.M. acknowledges support by a Cottrell Scholars Award, a program of Research Corporation for Science Advancement. N.S. acknowledges support from the National Science Foundation under Grant No. 2247194. K.E.R.-C. acknowledges support from the NSF Graduate Research Fellowship Program (No. DGE 125260) and a Ford Foundation Predoctoral Fellowship.

■ REFERENCES

(1) Masel, R. I.; Liu, Z.; Yang, H.; Kaczur, J. J.; Carrillo, D.; Ren, S.; Salvatore, D.; Berlinguette, C. P. An Industrial Perspective on Catalysts for Low-Temperature CO_2 Electrolysis. *Nat. Nanotechnol.* **2021**, *16* (2), 118−128.

(2) Birdja, Y. Y.; Pérez-Gallent, E.; Figueiredo, M. C.; Göttle, A. J.; Calle-Vallejo, F.; Koper, M. T. M. Advances and Challenges in Understanding the Electrocatalytic Conversion of Carbon Dioxide to Fuels. *Nat. Energy* **2019**, *4* (9), 732−745.

(3) Nielsen, D. U.; Hu, X.-M.; Daasbjerg, K.; Skrydstrup, T. Chemically and Electrochemically Catalysed Conversion of CO_2 to CO with Follow-up Utilization to Value-Added Chemicals. *Nat. Catal.* **2018**, *1* (4), 244−254.

(4) Dalena, F.; Senatore, A.; Marino, A.; Gordano, A.; Basile, M.; Basile, A. Methanol Production and Applications: An Overview. *Methanol*; Elsevier, 2018; pp 3−28.

(5) Wang, Y.-R.; Ding, H.-M.; Sun, S.-N.; Shi, J.; Yang, Yi.-L.; Li, Q.; Chen, Y.; Li, S.-L.; Lan, Y.-Q. Light, Heat and Electricity Integrated Energy Conversion System: Photothermal-Assisted Co-Electrolysis of CO2 and Methanol. *Angew. Chem., Int. Ed.* **2022**, *61* (50), No. e202212162.

(6) Todorova, T. K.; Schreiber, M. W.; Fontecave, M. Mechanistic Understanding of CO_2 Reduction Reaction (CO_2RR) Toward Multicarbon Products by Heterogeneous Copper-Based Catalysts. *ACS Catal.* **2020**, *10* (3), 1754−1768.

(7) Chang, X.; Li, J.; Xiong, H.; Zhang, H.; Xu, Y.; Xiao, H.; Lu, Q.; Xu, B. C−C Coupling Is Unlikely to Be the Rate-Determining Step in the Formation of C_{2+} Products in the Copper-Catalyzed Electrochemical Reduction of CO. *Angew. Chem.* **2022**, *134* (2), No. e202111167.

(8) Woldu, A. R.; Huang, Z.; Zhao, P.; Hu, L.; Astruc, D. Electrochemical CO_2 Reduction (CO_2RR) to Multi-Carbon Products over Copper-Based Catalysts. *Coord. Chem. Rev.* **2022**, *454*, No. 214340.

(9) Zhang, S.; Jing, X.; Wang, Y.; Li, F. Towards Carbon-Neutral Methanol Production from Carbon Dioxide Electroreduction. *ChemNanoMat* **2021**, *7* (7), 728−736.

(10) Yang, D.; Ni, B.; Wang, X. Heterogeneous Catalysts with Well-Defined Active Metal Sites toward CO_2 Electrocatalytic Reduction. *Adv. Energy Mater.* **2020**, *10* (25), No. 2001142.

(11) Wu, X.; Sun, J. W.; Liu, P. F.; Zhao, J. Y.; Liu, Y.; Guo, L.; Dai, S.; Yang, H. G.; Zhao, H. Molecularly Dispersed Cobalt Phthalocyanine Mediates Selective and Durable CO_2 Reduction in a Membrane Flow Cell. *Adv. Funct. Mater.* **2022**, *32* (11), No. 2107301.

(12) Soucy, T. L.; Dean, W. S.; Zhou, J.; Rivera Cruz, K. E.; McCrory, C. C. L. Considering the Influence of Polymer−Catalyst Interactions on the Chemical Microenvironment of Electrocatalysts for the CO_2 Reduction Reaction. *Acc. Chem. Res.* **2022**, *55* (3), 252−261.

(13) Zhu, M.; Ye, R.; Jin, K.; Lazouski, N.; Manthiram, K. Elucidating the Reactivity and Mechanism of CO_2 Electroreduction at Highly Dispersed Cobalt Phthalocyanine. *ACS Energy Lett.* **2018**, *3* (6), 1381−1386.

(14) Liu, Y.; McCrory, C. C. L. Modulating the Mechanism of Electrocatalytic CO_2 Reduction by Cobalt Phthalocyanine through Polymer Coordination and Encapsulation. *Nat. Commun.* **2019**, *10* (1), 1683.

(15) Rivera Cruz, K. E.; Liu, Y.; Soucy, T. L.; Zimmerman, P. M.; McCrory, C. C. L. Increasing the CO_2 Reduction Activity of Cobalt Phthalocyanine by Modulating the σ-Donor Strength of Axially Coordinating Ligands. *ACS Catal.* **2021**, *11* (21), 13203−13216.

(16) Ogura, K.; Takamagari, K. Electrocatalytic Reduction of Carbon Dioxide to Methanol. Part 2. Effects of Metal Complex and Primary Alcohol. *J. Chem. Soc., Dalton Trans.* **1986**, *8*, 1519−1523.

(17) Ogura, K.; Yoshida, I. Electrocatalytic Reduction of CO_2 to Methanol: Part 9: Mediation with Metal Porphyrins. *J. Mol. Catal.* **1988**, *47* (1), 51−57.

(18) Boutin, E.; Wang, M.; Lin, J. C.; Mesnage, M.; Mendoza, D.; Lassalle-Kaiser, B.; Hahn, C.; Jaramillo, T. F.; Robert, M. Aqueous Electrochemical Reduction of Carbon Dioxide and Carbon Monoxide into Methanol with Cobalt Phthalocyanine. *Angew. Chem., Int. Ed.* **2019**, *58* (45), 16172−16176.

(19) Boutin, E.; Salamé, A.; Merakeb, L.; Chatterjee, T.; Robert, M. On the Existence and Role of Formaldehyde During Aqueous Electrochemical Reduction of Carbon Monoxide to Methanol by

Cobalt Phthalocyanine. *Chem.—Eur. J.* **2022**, *28* (27), No. e202200697.
(20) Wu, Y.; Jiang, Z.; Lu, X.; Liang, Y.; Wang, H. Domino Electroreduction of CO_2 to Methanol on a Molecular Catalyst. *Nature* **2019**, *575* (7784), 639−642.
(21) Wu, Y.; Hu, G.; Rooney, C. L.; Brudvig, G. W.; Wang, H. Heterogeneous Nature of Electrocatalytic CO/CO_2 Reduction by Cobalt Phthalocyanines. *ChemSusChem* **2020**, *13*, 6296−6299.
(22) Kong, S.; Lv, X.; Wang, X.; Liu, Z.; Li, Z.; Jia, B.; Sun, D.; Yang, C.; Liu, L.; Guan, A.; Wang, J.; Zheng, G.; Huang, F. Delocalization State-Induced Selective Bond Breaking for Efficient Methanol Electrosynthesis from CO_2. *Nat. Catal.* **2023**, *6* (1), 6−15.
(23) Li, P.; Bi, J.; Liu, J.; Zhu, Q.; Chen, C.; Sun, X.; Zhang, J.; Han, B. In Situ Dual Doping for Constructing Efficient CO_2-to-Methanol Electrocatalysts. *Nat. Commun.* **2022**, *13* (1), 1965.
(24) Yang, H.; Wu, Y.; Li, G.; Lin, Q.; Hu, Q.; Zhang, Q.; Liu, J.; He, C. Scalable Production of Efficient Single-Atom Copper Decorated Carbon Membranes for CO_2 Electroreduction to Methanol. *J. Am. Chem. Soc.* **2019**, *141* (32), 12717−12723.
(25) Ren, S.; Joulié, D.; Salvatore, D.; Torbensen, K.; Wang, M.; Robert, M.; Berlinguette, C. P. Molecular Electrocatalysts Can Mediate Fast, Selective CO_2 Reduction in a Flow Cell. *Science* **2019**, *365* (6451), 367−369.
(26) Wang, M.; Torbensen, K.; Salvatore, D.; Ren, S.; Joulié, D.; Dumoulin, F.; Mendoza, D.; Lassalle-Kaiser, B.; Işci, U.; Berlinguette, C. P.; Robert, M. CO_2 Electrochemical Catalytic Reduction with a Highly Active Cobalt Phthalocyanine. *Nat. Commun.* **2019**, *10* (1), 3602.
(27) Jiang, Z.; Zhang, Z.; Li, H.; Tang, Y.; Yuan, Y.; Zao, J.; Zheng, H.; Liang, Y. Molecular Catalyst with Near 100% Selectivity for CO_2 Reduction in Acidic Electrolytes. *Adv. Energy Mater.* **2023**, *13* (6), No. 2203603.
(28) Yao, L.; Yin, C.; Rivera-Cruz, K. E.; McCrory, C. C. L.; Singh, N. Translating Catalyst−Polymer Composites from Liquid to Gas-Fed CO_2 Electrolysis: A CoPc-P4VP Case Study. *ACS Appl. Mater. Interfaces* **2023**, *15* (26), 31438−31448.
(29) Li, H.; Pan, Y.; Wang, Z.; Yu, Y.; Xiong, J.; Du, H.; Lai, J.; Wang, L.; Feng, S. Coordination Engineering of Cobalt Phthalocyanine by Functionalized Carbon Nanotube for Efficient and Highly Stable Carbon Dioxide Reduction at High Current Density. *Nano Res.* **2022**, *15*, 3056−3064.
(30) Su, J.; Musgrave, C. B.; Song, Y.; Huang, L.; Liu, Y.; Li, G.; Xin, Y.; Xiong, P.; Li, M. M.-J.; Wu, H.; Zhu, M.; Chen, H. M.; Zhang, J.; Shen, H.; Tang, B. Z.; Robert, M.; Goddard, W. A.; Ye, R. Strain Enhances the Activity of Molecular Electrocatalysts via Carbon Nanotube Supports. *Nat. Catal.* **2023**, *6*, 818−828.
(31) Ren, X.; Zhao, J.; Li, X.; Shao, J.; Pan, B.; Salamé, A.; Boutin, E.; Groizard, T.; Wang, S.; Ding, J.; et al. In-Situ Spectroscopic Probe of the Intrinsic Structure Feature of Single-Atom Center in Electrochemical CO/CO_2 Reduction to Methanol. *Nat. Commun.* **2023**, *14* (1), 3401.
(32) Rooney, C.; Lyons, M.; Wu, Y.; Hu, G.; Wang, M.; Choi, C.; Gao, Y.; Chang, C.-W.; Brudvig, G.; Feng, Z.; Wang, H. Active Sites of Cobalt Phthalocyanine in Electrocatalytic CO_2 Reduction to Methanol. *Angew. Chem.* **2023**, No. e202310623.
(33) Yao, L.; Rivera-Cruz, K. E.; Singh, N.; McCrory, C. C. L. Challenges and Opportunities in Translating Immobilized Molecular Catalysts for Electrochemical CO_2 Reduction from Aqueous-Phase Batch Cells to Gas-Fed Flow Electrolyzers. *Curr. Opin. Electrochem.* **2023**, *41*, No. 101362.
(34) Li, J.; Shang, B.; Gao, Y.; Cheon, S.; Rooney, C. L.; Wang, H. Mechanism-Guided Realization of Selective Carbon Monoxide Electroreduction to Methanol. *Nat. Synth.* **2023**, *2*, 1194.
(35) Ding, J.; Wei, Z.; Li, F.; Zhang, J.; Zhang, Q.; Zhou, J.; Wang, W.; Liu, Y.; Zhang, Z.; Su, X.; et al. Atomic High-Spin Cobalt(II) Center for Highly Selective Electrochemical CO Reduction to CH_3OH. *Nat. Commun.* **2023**, *14* (1), 6550.
(36) Farquhar, G. D.; Ehleringer, J. R.; Hubick, K. T. Carbon Isotope Discrimination and Photosynthesis. *Annu. Rev. Plant Physiol. Plant Mol. Biol.* **1989**, *40* (1), 503−537.
(37) Ren, H.; Kovalev, M.; Weng, Z.; Muhamad, M. Z.; Ma, H.; Sheng, Y.; Sun, L.; Wang, J.; Rihm, S.; Yang, W.; Lapkin, A. A.; Ager, J. W. Operando Proton-Transfer-Reaction Time-of-Flight Mass Spectrometry of Carbon Dioxide Reduction Electrocatalysis. *Nat. Catal.* **2022**, *5* (12), 1169−1179.
(38) Kramer, W. W.; McCrory, C. C. L. Polymer Coordination Promotes Selective CO_2 Reduction by Cobalt Phthalocyanine. *Chem. Sci.* **2016**, *7* (4), 2506−2515.

https://doi.org/10.1021/acscatal.3c04957
ACS Catal. 2024, 14, 366−372